11th World Congress on Computational Mechanics (WCCM XI)
5th European Conference on Computational Mechanics (ECCM V)
6th European Conference on Computational Fluid Dynamics (ECFD VI)
E. Oñate, J. Oliver and A. Huerta (Eds)

CFD MODELLING OF A BETA-TYPE STIRLING MACHINE

A. Della Torre[1], A. Guzzetti[1], G. Montenegro[1], T. Cerri[1], A. Onorati[1] and F. Aloui[2]

[1] Dip. di Energia, Politecnico di Milano, Via Lambruschini 4, I-20156 Milano, ITALY

[2] Université de Lille Nord de France, Laboratoire TEMPO, UVHC, F-59313 Valenciennes Cedex 9, FRANCE

Key words: Stirling engine, CFD modelling, Regenerator, Heat transfer, OpenFOAM

Abstract. In the last decades the Stirling technology has experienced a renewed interest in industry and academy, due to a wide range of possible applications for energy generation from renewable resources and waste-heat recovery. In this context, the adoption of CFD can give a substantial contribution to the development of this technology, since it allows to enhance the understanding of the physical phenomena occurring inside the machine and to provide useful guide-lines for its optimization.

In the present work CFD is applied to the simulation of a Beta-type Stirling machine. As preliminary step, in order to model the specific features of the machine, ad-hoc submodels were implemented on the basis of the open-source software OpenFOAM. In particular specific mesh motion strategies were developed for the description of the motion of the power piston and of the regenerator, in order to reproduce the variation of the volumes of the working spaces. Moreover, heat-transfer models were implemented for taking into account the presence of the heat source/sink of the cycle and the regenerator.

Simulations were performed on a small 300 cm^3 Beta Stirling configuration, installed at the laboratory TEMPO (University of Valenciennes, France) and instrumented with thermocouples and pressure transducers. Particular care was paid to the choice of the mesh resolution, in order to accurately describe the heat transfer inside the cold sink. The computational model was validated both on global quantities, such as the indicated power and heat transferred to the cold sink in a cycle, and on local measurement of temperature inside the machine.

The CFD model was applied in order to perform a parametric study involving different aspects related to the machine: regenerator properties, working fluid, mean cycle operating pressure and amount of heat introduced in the machine. Moreover, the effect of the law of variation of the volumes was investigated. In particular, an ideal law, not constrained by the need to impose the alternative piston/regenerator motion by means of a crankshaft, was applied showing improvements in terms of an higher efficiency of the cycle.

1 INTRODUCTION

In the last decades the Stirling technology has experienced a renewed interest in industry and academy, due to a wide range of possible applications for energy generation from renewable resources and waste-heat recovery. Compared to the other available technologies, a Stirling engine is characterized by different interesting aspects and strong points, such as: the possibility of operating with different heat sources, quiet operation with low level of noise and vibrations, low-emissions and the possibility of operating in absence of oxygen. On the other hand, the main limitations are related to the low specific power of the device, the slowness of the start-up phase and problems of mechanical reliability.

The ideal Stirling cycle is a close regenerative cycle in which the working fluid undergoes cyclic compression and expansion at different temperature levels. The cycle consists of four transformations: a) isothermal compression, b) isochoric regenerative heating, c) isothermal expansion and d) isochoric regenerative cooling. The ideal cycle is not only characterized by the same efficiency of the Carnot cycle (which represents the maximum efficiency theoretically achievable) but it exhibits also a higher specific work, due to the replacement of the isoenthropic transformations with the isochoric ones. However, the performances of the Stirling cycle are considerably penalized when it is realized in a real machine, because of different reasons: a) irreversibility of the real thermodynamic transformations, b) non-ideality of the real heat transfer transformations (isothermal heat addition/removal and regeneration), which in the ideal case should be performed under null temperature gradient and c) non-ideality related to mechanical/fluid-dynamic aspects, in particular related to the impossibility of imposing a discontinous motion to pistons/regenerator in practical applications [1, 2]. In particular, while the first category is common to all the thermal machines, the other two are typical of the devices working on the basis of a Stirling cycle. With regards to the regenerator different works, both theoretical and experimental, has been focused on its study and optimization in order to minimize the fluid-dynamic losses and to enhance the heat transfer and heat storage properties [3]. Moreover, with regards to the law of variation of volumes, different studies showed that the adoption of a crankshaft for imposing the alternative piston/regenerator motion leads to a significant reduction (40-60 %) of the area of the p-V cycle with respect to the ideal one.

The design of a Stirling device is particularly challenging, since different and complex physical phenomena are involved [4]. The theoretical models proposed in the literature, even if useful for the description and the understanding of the main operations of the machine, are, on the other hand, too much simplified to be applied for a detailed design of the device. For this reason, the practical conception and optimization of the machine layout is usually performed on a real prototype. In this context, the adoption of CFD tools can give a substantial contribution during the design phase of a new machine, since it allows to enhance the understanding of the physical phenomena providing useful guide-lines for its optimization. Moreover, CFD simulations allows to test different layouts and solutions, in

order to identify the more promising configuration to be built and experimentally tested.

2 LITERATURE REVIEW

Different approaches for the analysis of the Stirling cycle have been proposed in the literature. These models can be classified on the basis of their complexity as: zero order, first order, second order, third order and fourth order [2, 5, 6].

The zero order analysis, proposed by Beale in 1971, is the simplest approach and it was formulated in the attempt to establish a similitude among all the Stirling machines. It is based on the assumption that most of these engines operate under similar parametric conditions and, therefore, a general correlation between the power output and the main operating conditions (mean operating pressure and system frequency) and design parameters (swept volume) can be established. Due to the underlying simplifications of the approach, this analysis can be adopted only for a first attempt estimation of the performances of a machine.

The first order analysis was proposed in 1871 by Gustav Schmidt and for many years, almost until 1960, it remained as the reference model for Stirling engine developers; even today, because of its simplicity, this model is widely used for the initial sizing of the engines. The central attraction of this analysis is that it produces closed-form solutions for the performance which can be easily manipulated by the designer. The principal assumption of this model is that the hot space and the heater are at the uppest source temperature T_h, while the cold space and the cooler are both constant at the lowest sink temperature T_k. This assumption implies that the heat exchangers, including the regenerator, are perfectly effective and thus ideal. The engine is configured as series of five components representing respectively the compression space, the cooler, the regenerator, the heater and the hot space. Therefore any interconnecting volumes (e.g. ducts) will be included in the closer clearance volume. Each component is considered homogeneous and the thermophysical properties of the gas are modelled by means of the perfect gas equation of state. Moreover, it is assumed that friction losses, mechanical losses and fluid leakage are negligible over the entire engine. These ideal assumptions aim to simplify the problem, providing a quick way to estimate the relationship between the overall size of the engine and its power output. On the other hand, since most of the irreversibility sources are removed, this analysis can not be regarded as a tool for the design of the engine.

The second order analysis, as the first order, has the main purpose to determine the power output and efficiency of the machine by solving balances on a simplified system. The major improvement of the second order methods compared to the first order one, is that individual loss mechanism are identified and quantified, and therefore a more accurate prediction of the machine performances is available. In particular, the assumption of isothermal expansion and compression spaces is removed in a class of models which are usually identified as *adiabatic analysis*, among which should be cited the analysis proposed by Finkelstein (1960), Walker and Kahan (1965) and Lee and Berchowitz (1978). A further improvement of these models is then represented by some later works in which,

still maintaining the hypothesis of the previous analysis, various other losses are taken into account and studied. These methods can be classified as *quasi-stationary analysis* and were firstly introduced by Urieli and Berchowitz (1984) [2], and then widely used in the following years.

Third order methods, also known as nodal analysis, group all the 1D simulations of the Stirling engines and normally consist of three basic steps: (1) discretization of the engine geometry as a network of nodes and control volumes; (2) definition of the set of differential equations for the conservation of mass, momentum, and energy, which is closed by the equation of state for the working gas; (3) solution of the the system of differential equations by means of some adequate numerical method. Third order methods have been introduced with the purpose of considering simultaneously the many different complex processes coexisting in a Stirling engine, which were considered decoupled in the previous analysis. However, they still require empirical correlation to model the heat transfer coefficients and friction factors. These methods are more sophisticated and by far more expensive in computational effort with respect to the second order analysis: the domain is usually divided in many nodes and more equations have to be solved for each control volume, resulting in numerical stability problems. The set of partial differential equations can be solved with both finite difference methods or method of characteristics (Organ (1981) [1] and Larson (1981)). The third order methods can be applied for the simulation of the machine and the prediction of its performances, however they still presents some limitations for an application as design tool. In particular, they cannot account for the effects of the geometry on the internal flows as well as distributions of working fluid properties over longitudinal axes, thus resulting in an incomplete information for the design and the optimization of the machine components.

The last class of methods (fourth order) is represented by CFD analysis. Despite CFD is today widely applied in many fields (internal-combustion engines, aerodynamics, acoustics, etc), its application to Stirling engines is only recent and still suffers from many challenges. The Stirling machine is inherently a multi-physic and multi-scale system, involving different physical phenomena (fluid dynamics, heat transfer) occurring in different media (fluid and solid) at different length scales (from the machine scale to the small pore scale in the solid matrix of the regenerator) and having different characteristic times (convection and conduction). Moreover, the simulation has to take into account the motion of the moving parts of the machine and therefore mesh motion strategies are needed. An aspect which makes particularly challenging the application of the CFD to the optimization of Stirling machine is related to the intrinsic unsteady oscillatory nature of the flow inside the system. This peculiarity makes it difficult to address the simulation of a single component as an isolated system, because of the lack of the information required to impose realistic unsteady conditions at the boundaries. On the other hand, a simulation of the entire machine requires a long computational time to reach the convergence, since it is influenced by the characteristic time of the conduction in the solid components. In the literature there are few examples of works in which the unsteady behaviour of

single components are simulated [7], while most recent publications are moving towards the direction of modelling the whole engine at once, using both 2D or fully-3D models [8, 9, 10].

3 EXPERIMENTAL SETUP

The Stirling engine considered in this work (Figure 1) is a Beta-type machine [11], consisting of a piston, responsible for the work exchange during the expansion and compression phases, and a displacer, which moves the fluid between the hot and the cold spaces during the regeneration phases.

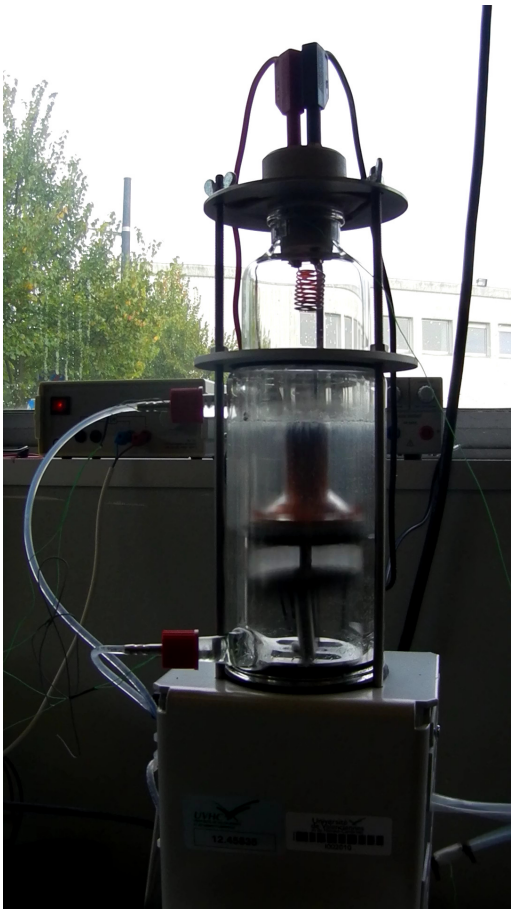

Figure 1: Stirling engine used for the validation of the model

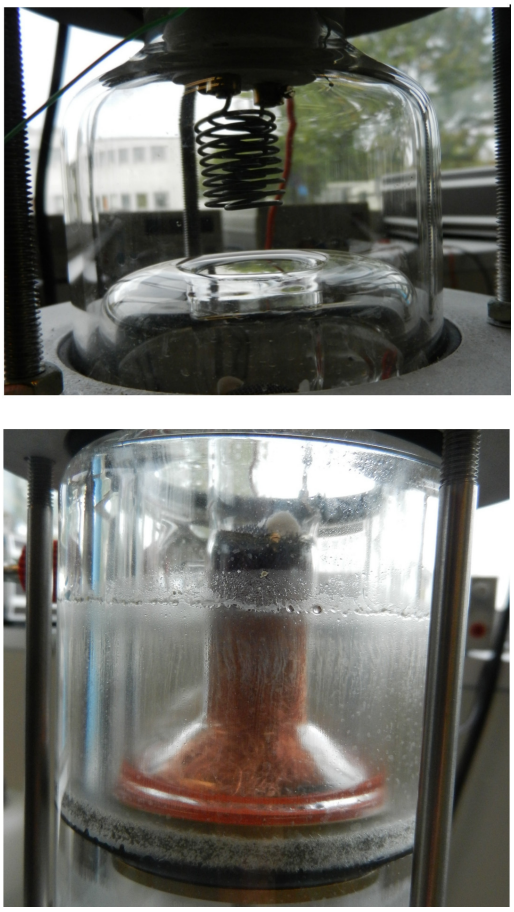

Figure 2: Particulars of the engine: electrical resistance and regenerator

This machine is a reversible device and can operate both as a prime mover or as receiver [12]. The hot source is represented by an electrical resistance located inside the hot room, whose power is imposed by means of a voltage regulator. The cold source consists of an open water circuit, which surrounds the cold room, and of an additional circuit realized

at the bottom of the displacer, in which the water flows through the con rod. The regenerator is inserted in the displacer piston and is made of a random fiber copper matrix; the matrix is shaped as a funnel and contained in an internal geometry, smaller then the cylinder dimensions, while the external geometry closes as a cylinder with the same width of the working spaces. The measuring apparatus is equipped with a pressure transducer, a volume transducer, a tachometer, a debimeter, and three thermocouples. The pressure transducer is located in the cold space and has 0.2 % of uncertainty in the measure. The volume transducer consists of a position sensor connected to the power piston which delivers a continuous tension signal, then internal volume is computed on the basis of the piston position. In order to monitor the temperatures of the working spaces, two thermocouples have been used, located respectively between the electrical resistance and the external wall in the hot room, and inside the power piston in the cold space. A differential thermocouple is used to measure the water temperature difference between the entrance and the end of the cooling circuit so that, measuring the water mass flow with the debimeter, it is possible to compute the average power exchanged by the cooling system. The working fluid used in the engine is air and is charged at ambient conditions by simply opening the top part of the cylinder. During the experimental tests, the machine was used as a prime mover, powered by the heat produced by the electrical resistance. Outside the hot room a radiative insulation was adopted, in order to reduce the radiative losses towards the surroundings. In addition no load was applied to the engine so that, when the functioning regime was reached, all the work output was balanced by the system friction losses.

After data acquisition a post-processing program was used to filter the rough signals and to compute the engine average performances. In particular the power exchanged in the cooling system was calculated as:

$$Q_{cold} = \dot{m}_{water} C_{p,water} \Delta T_{water}, \tag{1}$$

and work output was estimated integrating the pressure-volume diagram as:

$$W = \int p \, \mathrm{d}V. \tag{2}$$

Then, solving a global balance over the engine, the effective power Q_{hot} given to the fluid by the electrical resistance was determined as the sum of Q_{cold} and W. The geometrical characteristics of the engine and the operating conditions adopted during the experimental tests are summarized in Table 1.

4 CFD MODEL

In this section the implementation of a CFD model for the simulation of Stirling machine on the basis of the open-source finite volume code OpenFOAM will be described.

Table 1: Geometrical properties of the experimental engine

Hot space diameter $[mm]$	60
Hot space height $[mm]$	49.2
Displacer con rod length $[mm]$	100
Displacer stroke $[mm]$	48
Cold space diameter $[mm]$	60
Cold space height $[mm]$	35.7
Power piston con rod length $[mm]$	197
Power piston stroke $[mm]$	48
Regenerator inner diameter $[mm]$	22
Regenerator outer diameter $[mm]$	60
Regenerator height $[mm]$	59
Regenerator porosity $[-]$	0.79
Maximum machine volume cm^3	300
Minimum machine volume cm^3	160
Rotation speed rpm	235

4.1 Governing equations

In order to model the fluid-dynamic problem, the system of conservation equations for the generic continuum needs to be combined with the constitutive relations describing the properties of the specific medium. Considering a Newtonian compressible single-phase fluid, the mathematical set of governing equations consists of:

- Continuity equation, which states the conservation of mass:

$$\frac{\partial \rho}{\partial t} + \nabla \cdot (\rho \mathbf{U}) = 0 \tag{3}$$

- Navier-Stokes equation, derived from the conservation of momentum (linear and angular):

$$\begin{aligned} &\frac{\partial \rho \mathbf{U}}{\partial t} + \nabla \cdot (\rho \mathbf{U}\mathbf{U}) = \rho \mathbf{g} - \nabla \left(p + \frac{2}{3}\mu \nabla \cdot \mathbf{U} \right) \\ &+ \nabla \cdot \left[\mu \left(\nabla \mathbf{U} + \nabla \mathbf{U}^T \right) \right] + \mathfrak{R} \end{aligned} \tag{4}$$

- Energy equation:

$$\begin{aligned} &\frac{\partial \rho e}{\partial t} + \nabla \cdot (\rho e \mathbf{U}) = \rho \mathbf{g} \mathbf{U} - \nabla \cdot (p \mathbf{U}) \\ &- \nabla \cdot \left[\frac{2}{3}\mu \left(\nabla \cdot \mathbf{U} \right) \mathbf{U} \right] + \nabla \cdot \left[\mu \left(\nabla \mathbf{U} + \nabla \mathbf{U}^T \right) \mathbf{U} \right] \\ &+ \nabla \cdot (\lambda \nabla T) + \rho Q + Q^{s \to f} \end{aligned} \tag{5}$$

This set of equations is close by means of the perfect gas equation of state. On the other hand, when a solid medium is considered, the set of governing equations reduces to the energy conservation equation, which describes the conductive heat-transfer process:

$$\frac{\partial \rho c_s T}{\partial t} = \lambda_s \nabla T + \rho Q + Q^{f \to s}. \tag{6}$$

Eqn. 6, together with Eqns. 3 - 5, allows the description of the physics of porous systems including fluid and solid phases, e.g. the conjugate heat transfer process occurring in the regenerator matrix of the Stirling machine. In this case, the interaction between the two phases is described by means of specific sub-models introduced for source terms $\mathfrak{R}$, $Q^{s \to f}$ and $Q^{f \to s}$.

4.2 Mesh generation and mesh motion

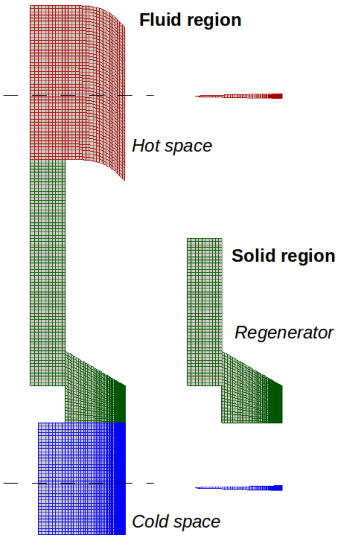

Figure 3: Computational meshes for the fluid and solid regions. The different motion zones are highlighted: cold space (blue), hot space (red) and regenerator (green).

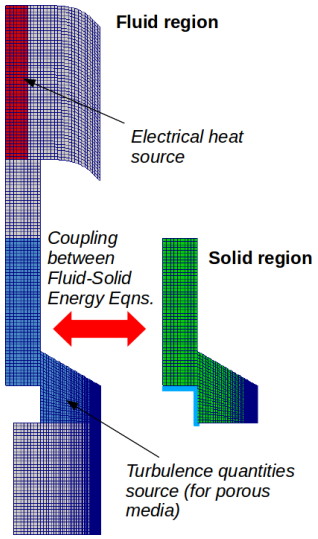

Figure 4: Definition of the cell zones on which the source terms needed for the simulation of the machine are applied.

The Stirling machine configuration considered in this work exhibits an axial-symmetric geometry, allowing to reduce the size of the problem resorting to a wedge-type discretization. The mesh was generated by means of a parametric script which, on the basis of the main geometrical parameters of the machine, creates a structured hexaedral mesh as shown in Fig. 3. The mesh motion was handled by means of the implementation of a flexible framework which allows to define an arbitrary number of moving zones and to prescribe their motion according to user-defined motion laws. In Fig. 3 the three moving zones needed for the modelling of this Beta-type machine are highlighted, namely the hot

space (red), the cold space (blue) and the regenerator (green). The motion of each space is specified by defining the direction and the displacement for the top and bottom points of the zone. The position of the internal points of the zone is prescribed interpolating between the position of the boundary points. The motion law can be either the law of a piston connected to a crank through a connecting rod or be arbitrarily specified in terms of position as a function of the angle (Fig. 13).

4.3 Simulation approaches: single-region and multi-region

The simulation of the heat transfer between fluid and regenerator is the most critical aspect related to the simulation of a Stirling engine. As matter of the fact, the amount of energy transferred during the regeneration phase of the each cycle is considerable and ranges between 3 to 40 times the total heat introduced in the heater. In order to describe this phenomenon, two different simulation approaches can be adopted. The first approach consists of assuming the temperature distribution in the solid matrix as a-priori known and constant during the simulation. In this way the governing equations (3 - 5) are solved for the single fluid phase, while no balance equation is solved for the solid. The second, more accurate, approach consists of adopting two different solution domains, one for the fluid and one for the solid phase, which the whole set of Eqns 3-6 is solved on. Where fluid and solid phases coexist, e.g. in the porous matrix of the regenerator, the computational grids overlap and models are introduced for taking into account their interactions (Fig. 4). In this way the temperature distribution in the solid matrix is determined by the global energy balance of the coupled fluid-solid system.

4.4 Sub-models for the simulation of the regenerator

In order to address the macro-scale simulation of the regenerator, suitable sub-models for the permeability and the inter-phase heat transfer of the porous media have to be included:

1. **Permeability model:** The permeability model is included in the momentum equation by means of the resistance source term $\mathfrak{R}$. Its effective value depends on the properties of the micro-structure and the instantaneous fluid-dynamics conditions. If the flow resistance is expressed in terms of a friction factor correlation, the momentum equation can be closed by means of the following expression:

$$\mathfrak{R} = \frac{1}{2}\frac{\rho}{d_c} C_f \mathbf{U}. \tag{7}$$

In this work we adopted the correlation proposed by Gedeon and Wood [13]:

$$C_f = \frac{129}{Re} + 2.91 Re^{-0.103}. \tag{8}$$

2. **Inter-phase heat transfer model:** This is included as source term in the energy equations of fluid and/or solid phase. Its value depends on the instantaneous fluid-dynamics conditions and on the averaged temperatures of the phases. As for the case of the resistance, it can be evaluated by means of a suitable relationship expressing the dependency of the heat transfer on the Re and on Pr numbers:

$$Q^{s \to f} = -Q^{f \to s} = Nu \, \frac{\lambda_f}{d_c} \, \sigma \, V \, (T_s - T_f) \, , \tag{9}$$

where the following correlation has been adopted (Gedeon and Wood [13]):

$$Nu = 0.51 + 0.4 Re^{0.66}. \tag{10}$$

4.5 Models for the heat source and the cold sink

In order to describe the heat exchange mechanisms at the hot and the cold spaces, specific modelling strategies were adopted. In particular, the modelling of the electrical resistance located in the hot space was addressed introducing a volume source term on the energy equation (Eqn. 5). The source term is applied to a zone of cells defined in the region where the electrical resistance is located (Fig. 4). A limitation on the maximum power introduced in the fluid is applied, to ensure that the temperature in the cell zone does not exceed a maximum value. When this situation occurs, energy is temporarily accumulated and introduced in the fluid system only when temperature returns below the maximum limit. In this way, the effect of energy accumulation, which occurs in the metallic wire of the resistance and preserves the temperature to rise in case of low speed gas flow (e.g. at the top dead center), is reproduced. The removal of the heat at the cold sink is performed by means of a water circuit, which cools the walls of the cold cylinder and the bottom part of the regenerator. In this cases, a fixed temperature condition was imposed at the boundaries of the fluid and solid regions. In particular, on the fluid region, a mesh having a refined boundary layer was adopted, in order to accurately describe the wall heat transfer.

4.6 Turbulence model

The most common way to describe turbulence phenomena in CFD problems is to use a turbulence model. In turbulence modelling, an averaging operation is applied to the Navier-Stokes equations to form an equivalent set of equations for the averaged flow quantities. This leads to the Reynolds Averaged Navier Stokes (RANS) equations, which present an additional term in the momentum equation, the Reynolds Stress term. The Reynolds Stress term represents the effect of the stochastic component of the flow on the mean flow, and can be replaced by a turbulence model to achieve closure. In this work the k-ω SST model, proposed by Menter [14], has been applied. This is a widely-adopted two-equation eddy-viscosity model based on the solution of the transport equations for

two quantities, namely turbulent kinetic energy and specific dissipation rate, and can be adopted as a low-Re model without any extra damping functions. However, when a turbulence model is applied to describe the flow characteristics through a porous media (e.g. through the regenerator) specific sub-models needs to be introduced. As a matter of fact, a turbulent flow entering in a porous media experiences a drastic change of its turbulent properties, due to the fact that the integral length-scale reduces of orders of magnitude, becoming similar to the pore dimension of the media. In most practical applications, when the flow velocity in the porous media is kept low in order to maintain the pressure drop within an acceptable range of values, the flow regime in the media is laminar. In this case, the presence of the porous media determines the re-laminarization of the turbulent flow passing through that. This is particularly important in a Stirling machine since it means that the turbulence generated in one space is not transferred into the other and, therefore, the positive effect of the turbulence to promote the heat transfer with the walls of the spaces is minimized. In order to take into account this phenomenon a simplified sub-model has been introduced. It consists of an additional source term added in the specific dissipation rate equation, which has the effect to determine the re-laminarization of the flow passing through the porous media.

5 NUMERICAL SIMULATIONS AND VALIDATION

In this section the developed model will be firstly validated against experimental data and then applied in order to perform a study on the machine design parameters and to investigate the aspects related to the adoption of an ideal law of variation of the volumes.

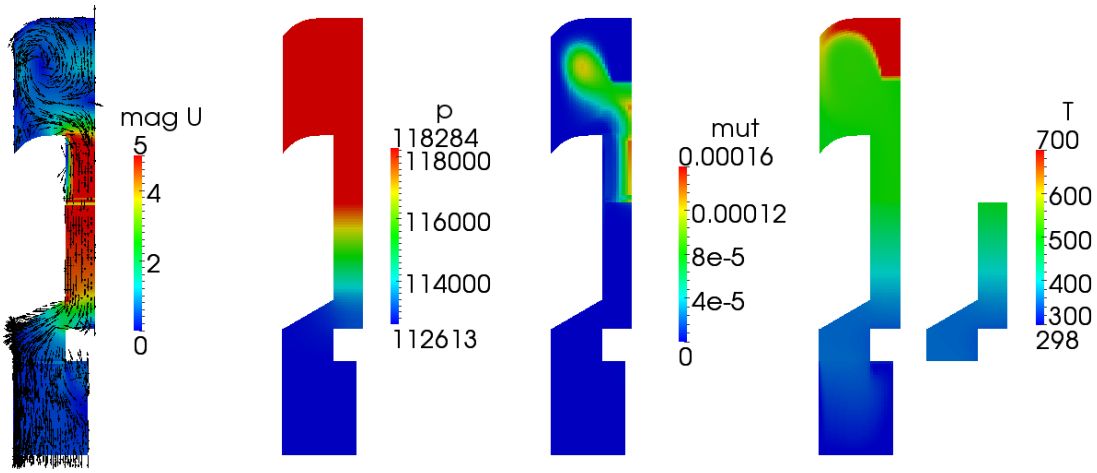

Figure 5: Fields during the isochoric cooling regenerative transformation. From left to right: velocity, pressure, turbulent viscosity and temperature (on both fluid and solid domain).

Figures 5 and 6 shows the fields of different fluid-dynamics quantities during the regeneration phases, when the axial motion of the displacer forces the fluid to move from one of

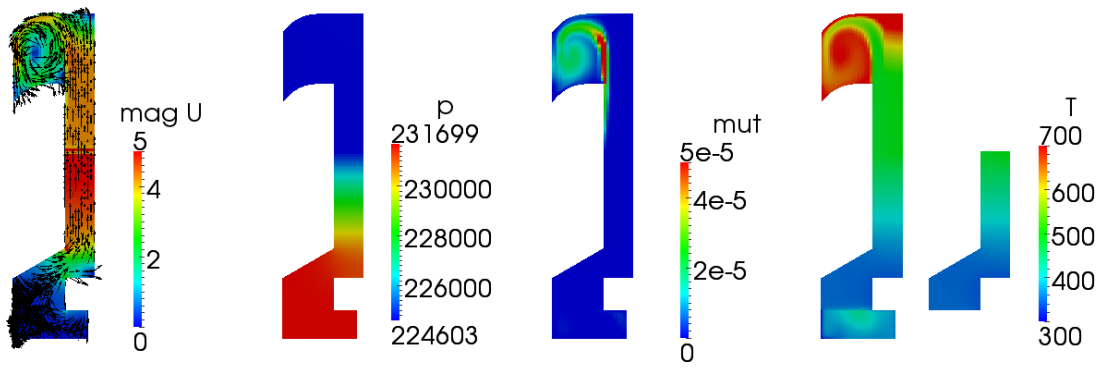

Figure 6: Fields during the isochoric heating regenerative transformation. From left to right: velocity, pressure, turbulent viscosity and temperature (on both fluid and solid domain).

the two spaces to the other passing through the regenerator. During the isochoric cooling transformation (Fig. 5) the displacer moves from the bottom to the top, determining the motion of the fluid towards the cold space. As a result of the flow through the porous media, a pressure difference between the hot and cold spaces is originated. Moreover the regenerator, whose temperature varies linearly along its axis, accumulates energy from the fluid, cooling it to a temperature close to the one of the cold space. The CFD models takes into account also the re-laminarization of the turbulent flow which passes through the porous regenerator: it can be noticed that the turbulent viscosity drops to a very low value during the passage through the displacer. The analogous isochoric heating transformation is illustrated in Fig. 6: in this case the energy accumulated in the regenerator matrix during the previous transformation is given back to the fluid which passes from the bottom to the top. Simulations were run with the multi-region approach until a convergency criteria for different global quantities averaged over the cycle (e.g. power, heat at the cold sink, averaged temperature in the hot/cold spaces and the regenerator) is satisfied. Convergency is usually reached after the simulation of 300-600 cycles (1-2 mins of simulated time).

5.1 Model validation

The computational model was validated both on global quantities, such as the power and heat transferred to the cold sink in a cycle, and on local measurements of temperature in the machine. In Fig. 7 the comparison of measured and computed p-V cycles is reported, showing a satisfactory agreement.

Moreover, in Fig. 8 the p-V diagram for the expansion space and the compression space are shown, along with the global cycle plotted using the averaged pressure and the total machine volume. Additional validation quantities are reported in Table 2. The mechanical power of the device was experimentally determined from the pressure probed in the cold space; for this reason are reported both the mechanical power evaluated using the pressure calculated in the same position $P_{mech,cold}$ and the effective mechanical

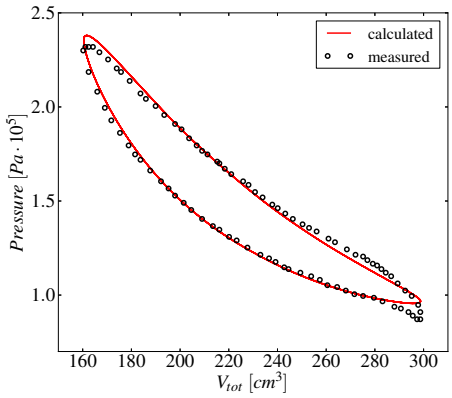

Figure 7: Base case: comparison of measured and computed p-V cycle.

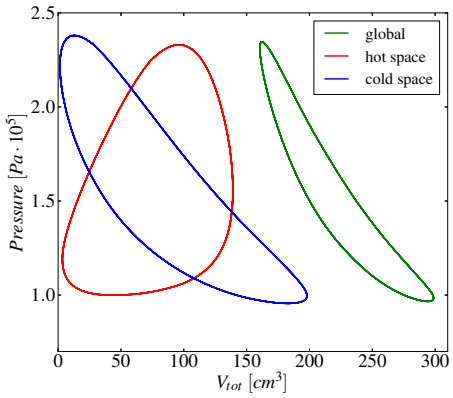

Figure 8: p-V cycles for the base case: compression space, expansion space and global machine cycle.

Table 2: Comparison between measurements and simulation results.

Quantity	**Measurement**	**Simulation**
Power cooling system Q_{cold} [W]	84.9	82.9
Mechanical power $P_{mech,cold}$ [W]	13.2	14.2
Mechanical power P_{mech} [W]	-	9.82
Hot temperature $T_{hot,rad}$ [W]	818	-
Hot temperature T_{hot} [W]	692	681

power P_{mech} determined as a difference between the power of the expansion space and the compression space. With regards to the temperature probed in the hot space, the experimental measurement $T_{hot,rad}$ is affected by the influence of the radiative heat transfer. As a matter of fact, the thermocouple is not shielded against radiation and the hot source (electrical resistance) reaches high temperature during the operation of the machine. In order to take into account this measurement error a simple analytical model has been developed, leading to the estimation of the fluid temperature T_{hot} reported in the table. Considering this estimation, the temperature of the fluid calculated at the transducer location shows a reasonable value.

5.2 Parametric study

Once validated, the model was adopted in order to investigate the effects of different design parameters and operating conditions on the machine performances, as summarized in Table 4. As previously said, the regenerator is the key component for the optimization of the performances of a Stirling device. In particular, an important property of the regenerator is the thermal conductivity of the porous matrix, since it influences the efficiency losses related to the heat transfer from the hot source to the cold source. In an ideal

Table 3: Parametric study: simulation results.

Parameter	**Value**	$\mathbf{P_{mech}}[W]$	$\mathbf{Q_{cold}}[W]$	$\mathbf{Q_{hot}}[W]$	$\mathbf{T_{cold}}[K]$	$\mathbf{T_{hot}}[K]$
Base case		9.8	82.9	92.7	314.6	681.8
Conductivity	10	18.8	64.4	83.2	315.8	763.0
$[W/(m^2K)]$	100	1.3	91.6	92.9	318.3	608.2
Fluid	Helium	10.2	82.5	92.6	320.4	623.8
Pressure $[Pa \cdot 10^5]$	0.7	10.2	72.1	82.3	308.0	722.9
	1.5	2.2	90.5	92.7	326.4	576.3
$\mathbf{Q_{hot}}$ $[W]$	50	-4.8	54.5	49.6	329.3	527.5
	150	23.7	109.1	132.8	304.5	894.2
Motion	Ideal	10.8	82.8	93.6	359.3	586.2

Table 4: Parametric study: calculated efficiencies.

Parameter	**Value**	$\eta_{\mathbf{Carnot}} = \mathbf{1} - \frac{\mathbf{T_{cold}}}{\mathbf{T_{hot}}}$	$\eta_{\mathbf{I}} = \frac{\mathbf{P_{mech}}}{\mathbf{Q_{hot}}}$	$\eta_{\mathbf{II}} = \frac{\eta_{\mathbf{I}}}{\eta_{\mathbf{Carnot}}}$
Base case		0.54	0.11	0.20
Conductivity	10	0.59	0.23	0.38
$[W/(m^2K)]$	100	0.48	0.01	0.03
Fluid	Helium	0.49	0.11	0.23
Pressure $[Pa \cdot 10^5]$	0.7	0.57	0.12	0.22
	1.5	0.43	0.02	0.06
$\mathbf{Q_{hot}}$ $[W]$	50	0.38	-0.10	-0.26
	150	0.66	0.18	0.27
Motion	Ideal	0.39	0.12	0.30

machine the axial conductivity of the regenerator should be null, in order to minimize this loss. On the other hand, in real applications, the effective thermal conductivity of a typical porous matrix is sensibly lower with respect to the conductivity of the material which it is made of, making it possible to reach a good compromise between a high inter-phase heat transfer and a low axial thermal conductivity. In Fig. 9 the p-V cycles computed in the case of different effective conductivity of the porous matrix is shown. It can be seen that the area of the global cycle increases as the conductivity decreases. This is due to the fact that, as reported in Table 4, a higher temperature is reached in the hot space because of the heat losses towards the cold space are lower. This results in an higher first law efficiency η_I of the cycle, since the temperature difference between the spaces increases, but also in a higher second law efficiency η_{II}, because of the reduced irreversibility source. On the other hand, the adoption of helium as working fluid instead of air (Fig. 10) does not have significant impact on the thermodynamic cycle for this type of machine.

Moreover, the effect of the variation of the mean pressure of the cycle was investigated.

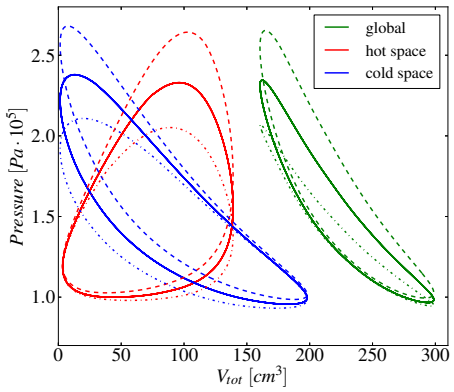

Figure 9: Effects of a variation of the effective conductivity $k_{reg,eff}$ of the regenerator: base case, $k_{reg,eff} = 30\,W/(m^2K)$ (continuos line), $k_{reg,eff} = 10\,W/(m^2K)$ (dashed line), $k_{reg,eff} = 100\,W/(m^2K)$ (dotted line).

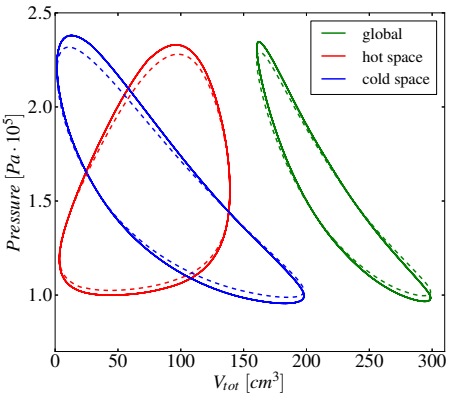

Figure 10: Effects of a variation of the working fluid: base case, air (continuos line) and helium (dashed line).

This parameter controls the mass of working fluid which operates in the cycle and is usually adopted in practical application in order to modify the load, and therefore the mechanical power output, of the machine. A higher mechanical power is therefore obtained by means of the combined increase of both mean pressure and heat power introduced in the hot space. In the graph reported in Fig. 11 the mean pressure of the cycle is varied keeping constant the heat power transferred in the hot space. In this case, when the mass is increased keeping constant the amount of heat introduced, the temperature of the hot space decreases, determining a reduction of the weight of the expansion work over the compression work. The area of the resulting global cycle is reduced compared to the base case, and since the heat introduced is the same, also the efficiency η_I drops. Conversely, the reduction of the mean pressure determines an increase of the power output, since the increase of the temperature difference between hot and cold end results in a higher efficiency η_I.

Finally the effect of the amount of heat introduced in the device was investigated. Fig. 12 shows that the increase of the heat determines a higher power output of the machine. Moreover the efficiency η_I increases, since the weight of work of the compression space over the global work decreases. On the contrary, a reduction of the heat power at the hot end determines a reduction of the work of the expansion space, which can become not sufficient to overcome the compression work, resulting in a negative power output of the machine.

5.3 Study on the adoption of an ideal law of variation of the volumes

As last part of the work, the adoption of an arbitrary law of variation of the volumes, removing the constrain of imposing the alternative piston/regenerator motion by means

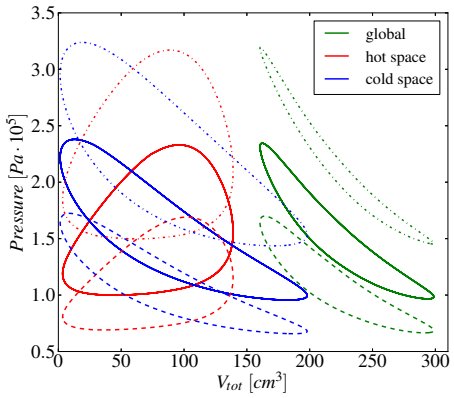

Figure 11: Effects of a variation of the mean pressure of the cycle: base case, $10^5\,Pa$ (continuos line), $0.7 \cdot 10^5\,Pa$ (dashed line), $1.5 \cdot 10^5\,Pa$ (dotted line).

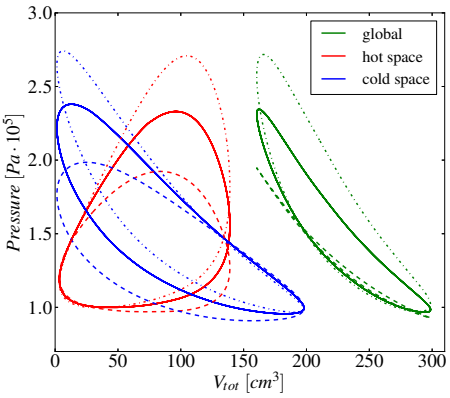

Figure 12: Effects of a variation of the amount of heat introduced in the hot space Q_{hot}: base case, $Q_{hot} = 93\,W$ (continuos line), $Q_{hot} = 50\,W$ (dashed line), $Q_{hot} = 150\,W$ (dotted line).

of a crankshaft, was investigated. The motion law of the power piston and the regenerator was designed in such a way to impose the ideal law of variation of the volumes according to the theoretical Stirling cycle. In Fig. 13 the ideal motion laws are compared to the pseudo-sinusoidal ones considered for the real device. The combination of the two laws for the piston and the displacer allows to obtain a variation of the global volume restricted to the single expansion/compression phases, while the regeneration transformations are performed keeping the volume as constant. As shown in Fig. 14, the shape of the resulting p-V cycle is similar to the theoretical one. On the other hand, it can be seen that the power output is not significantly higher if compared to the one predicted for machine with the real motion laws. This is due to the particular engine configuration, which is designed and optimized in order to adopt a sinusoidal motion law. As matter of fact, in the ideal Stirling cycle the cooling in the cold space should be performed during the compression phase. However, this implies to have a cooling heat exchanger located in the compression space (like the electrical heat source adopted at the hot end), which is usually not feasible from a construction point of view. For this reason, in the experimental device considered in this work, an heat exchanger located at the bottom of the regenerator was adopted. Combining the sinusoidal motion of the compression piston with the sinusoidal motion of the regenerator is it possible, in the experimental device, to promote the convective heat transfer during the compression phase. On the other hand, when an ideal motion law is applied, the regenerator remains at a fixed position during the compression phase and the cooling effect of the heat exchanger is significantly reduced. As can be seen in Table 4 the average temperature in the cold space is around 40 K higher with respect to the base case, implying also an increase of the compression work. On the other hand, considering the second law efficiency η_{II}, it is possible to argue that the ideal motion introduces less irreversibility with respect to the sinusoidal motion. This means that, for

the ideal motion, an optimization of the heat exchange during the cooling phase would lead also to a significant gain in terms of mechanical power output and first law efficiency η_I.

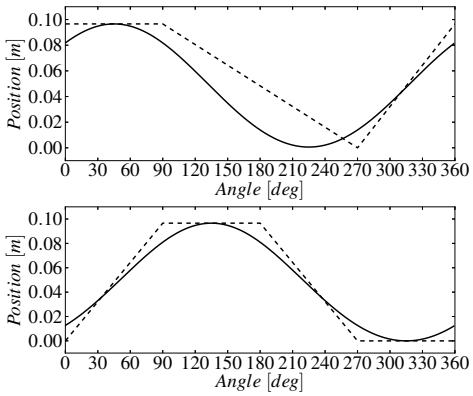

Figure 13: Motion laws adopted for the power piston (bottom) and the displacer (top): sinusoidal law (continous line) and ideal law (dashed line).

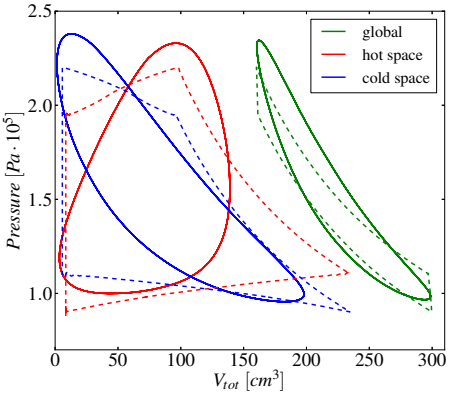

Figure 14: Effects of the law adopted for the motion of the piston and the displacer: base case, sinusoidal law (continuos line) and ideal law (dashed line).

6 CONCLUSIONS

In this work a CFD model for the simulation of a generic Beta-type Stirling engine has been developed on the base of the finite volume open-source code OpenFOAM. Different sub-models has been implemented in order to take into account particular features of this machine, related to mesh motion, heat transfer, turbulence modelling and treatment of porous media. The model has been successfully validated on the case of a small 300 cm^3 Beta Stirling configuration, by means of comparison of both global quantities, such as the power and heat transferred to the cold sink in a cycle, and of local measurement of temperature in the machine. Once validated, the model was applied to perform a parametric study on different parameters of the machine, such as regenerator properties, working fluid, mean cycle operating pressure and amount of heat introduced at the hot end. Moreover the effect of the adoption of an ideal law for the motion of the power piston and the displacer was investigated. The results provided by the CFD model for these cases seems to be reasonable and in agreement to what expected on the basis of the existing theoretical models.

REFERENCES

[1] A.J. Organ. Thermodinamics and Gas Dynamics of the Stirling Cycle Machine. Cambridge, Cambridge University Press, 1992.

[2] I. Urieli and D.M. Berchowitz. Stirling Cycle Engine Analysis. Bristol, Adam Hilger Ltd, 1984.

[3] R. Gheith, F. Aloui, M. Tazerout, and S. Ben Nasrallah. Experimental investigations of a gamma stirling engine. Int. J. Energy Res., 2012.

[4] W.R. Martini. Stirling engine design manual. NASA-CR-158088, January 1983.

[5] N.C.J. Chen and F.P. Griffin. A review of stirling engine mathematical models. Oak Ridge National Laboratory, August 1983.

[6] R.W. Dyson, S.D. Wilson, and R.C Tew. Review of computational stirling analysis methods. NASA/TM-2004-213300, October 2004.

[7] M.B. Ibrahim, Z. Zhang, Rong Wei, T.W. Simon, and D. Gedeon. A 2-d cfd model of oscillatory flow with jets impinging on a random wire regenerator matrix. In Energy Conversion Engineering Conference, 2002. IECEC '02. 2002 37th Intersociety, pages 511–517, July 2002.

[8] Z. Zhang and M. Ibrahim. Development of cfd model for stirling engine and its components. 2nd International Energy Conversion Engineering Conference, 2004.

[9] K. Mahkamov. Design improvements to a biomass stirling engine using mathematical analysis and 3d cfd modeling. J. Energy Resour. Technol., 128(3), September 2005.

[10] R.W. Dyson, S.M. Geng, R.C. Tew, and M. Adelino. Towards fully three-dimensional virtual stirling convertors for multi-physics analysis and optimization. Engineering application of computational fluid mechanics, 12(1), 2008.

[11] G. Walker. Stirling-Cycle machines. Oxford University Press, 1973.

[12] R. Gheith, F. Aloui, and S. Ben Nasrallah. Experimental study of a beta stirling thermal machine type functioning in receiver and machine modes. Journal of Applied Fluid Mechanics, 2011.

[13] D. Gedeon and J.G. Wood. Oscillating-flow regenerator test rig: hardware and theory with derived correlations for screens and felts. NASA CR-198442, 1996.

[14] F. Menter and T. Esch. Elements of Industrial Heat Transfer Prediction. 16th Brazilian Congress of Mechanical Engineering (COBEM), 2001.